SIAM J. APPL. MATH.
Vol. 78, No. 2, pp. 719–741

DOUBLY STOCHASTIC POISSON MODEL OF FLAGELLAR LENGTH CONTROL*

PAUL C. BRESSLOFF† AND BHARGAV R. KARAMCHED†

Abstract. We construct and analyze a stochastic model of eukaryotic flagellar length control. Flagella are microtubule-based structures that extend to about 10 μm from the cell and are surrounded by an extension of the plasma membrane. Flagellar length control is a particularly convenient system for studying organelle size regulation since a flagellum can be treated as a one-dimensional structure whose size is characterized by a single length variable. The length of a eukaryotic flagellum is important for proper cell motility, and a number of human diseases appear to be correlated with abnormal flagellar lengths. Flagellar length control is mediated by intraflagellar transport (IFT) particles, which are large motor protein complexes within a flagellum that transport tubulin (the basic building block of microtubules) to the tip of the flagellum. The critical length of the flagellum is thus thought to be determined by the dynamical balance between length-dependent transport and assembly of microtubules and length-independent disassembly at the tip. In our model we assume that IFT particles are injected into a flagellum according to a Poisson process, with a rate that depends on a second stochastic process associated with the binding and unbinding of IFTs to sites at the base of the flagellum. The model is thus an example of a doubly stochastic Poisson process (DSPP), also known as a Cox process. We use the theory of DSPPs to analyze the effects of fluctuations on IFT and show how our model captures some of the features of experimental time series data on the import of IFT particles into flagella. We also indicate how DSPPs provide a framework for developing more complex models of IFT.

Key words. Poisson processes, cellular length control, flagellar, generating functionals

AMS subject classifications. 82C31, 92C37

DOI. 10.1137/16M110811X

1. Introduction.

A fundamental issue in cell biology is how cells regulate the size of their organelles [29]. There are a number of different mechanisms utilized by cells, including molecular rulers in the case of bacteriophage tails [16], sensor-based size control in the case of *salmonella* flagellar motor filaments [17], and a variety of dynamical mechanisms where size is determined by the balance between assembly and disassembly of some subcellular structure. Probably the best-studied model system controlled dynamically is a eukaryotic flagellum [27, 33, 28, 37, 24, 25, 20, 31], which is a microtubule-based structure that protrudes from the cell membrane up to about 10 μm in length. A flagellum can effectively be treated as a one-dimensional structure whose size is characterized by a single length variable. This makes it a particularly convenient system for studying organelle size regulation. Moreover, eukaryotic flagella play an important role in cell motility, and various human diseases appear to be correlated with flagellar length abnormalities.

The fundamental building block (monomer) of microtubular filaments is the protein tubulin. Experimental measurements of tubulin turnover in eukaryotic flagella combined with various imaging studies have established that the assembly of microtubules is mediated by molecular motor complexes known as intraflagellar transport

*Received by the editors December 15, 2016; accepted for publication (in revised form) November 28, 2017; published electronically March 8, 2018.
http://www.siam.org/journals/siap/78-2/M110811.html
Funding: The first author's work was supported by the National Science Foundation (DMS-1613048).
†Department of Mathematics, University of Utah, Salt Lake City, UT 84112 (bressloff@math.utah.edu, karamche@math.utah.edu).

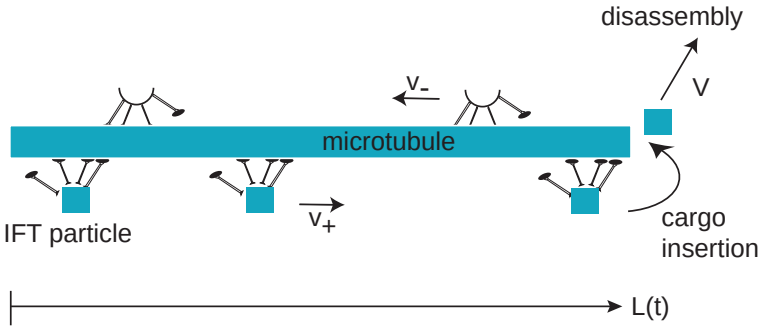

FIG. 1. *Schematic diagram of intraflagellar transport (IFT). Each IFT particle carries tubulin to the tip of a flagellum at a speed v_+, where it is released and attached to the microtubule (assembly), and the IFT particle returns to the base at a speed v_-. Disassembly occurs independently of IFT transport at a speed V.*

(IFT) particles or trains, which carry tubulin to the tip of the flagellum, where assembly and disassembly of microtubules take place [33]. A schematic diagram of IFT transport is shown in Figure 1. As a flagellum grows, each IFT particle has to travel a longer distance to deliver tubulin at the tip of the flagellum, which implies that the corresponding rate of assembly will decrease with length. On the other hand, it is found experimentally that the rate of disassembly is length independent, suggesting that there exists a critical length where the rates of assembly and disassembly are balanced. More specifically, suppose that each IFT particle moves at a mean speed v. (Experimentally, one finds that the anterograde speed to the tip is $v_+ \sim 1.5$ μm/s, whereas the retrograde speed away from the tip is $v_- \sim 2$ μm/s due to a lighter load.) Assuming that an IFT particle is immediately reinjected into the flagellum when it returns to the base, and if the time spent at the tip is neglected, then the time between tubulin deliveries is $2L/v$, where v is the harmonic mean. If the number N of IFT particles is fixed, then the mean rate of change of length L is given by the simple equation [27]

$$\frac{dL}{dt} = \frac{avN}{2L} - V, \tag{1.1}$$

where a is the size of a single tubulin molecule and V is the speed of disassembly. Equation (1.1) has a unique stable equilibrium given by $L^* = avN/2V$. Using the experimentally based values $N = 10$, $v = 2$ μm/s, $L^* = 10$ μm, and $V = 0.01$ μm/s, the effective precursor protein size is estimated to be $a \approx 10$ nm. (A stochastic version of a model for intraflagellar transport has also been developed using the theory of continuous time random walks [3].)

However, the above model is oversimplified. In particular, there is growing experimental evidence that the flux of IFT particles into the flagellum is regulated by the amount of accumulated IFT particles at the base of the flagellum [24, 37, 22, 25]. Moreover, recent photobleaching studies have shown that there is constant turnover of IFT particles within flagella, presumably through the exchange of IFT particles between the basal body and the cytoplasm [25]. An emerging picture is that IFT particles enter the flagellum through the flagellar pore, a membrane-spanning structure at the base of the flagellum that may be homologous to a nuclear pore. (The latter regulates the exchange of macromolecules between a cell's cytoplasm and the nucleus.) There is also a microtubule-organizing center known as the *basal body*, which

anchors the flagellar microtubules at the plasma membrane and integrates them with the cytoplasmic microtubules. IFT proteins dock around the basal body and assemble into IFT particles or trains prior to entering the flagellum [9]. It appears that the rate at which IFT particles enter the flagellum depends on the amount of docked IFT particles in the basal body, with faster-growing flagella having more localized IFT particles [24, 37]. This suggests that there is some length-dependent mechanism for regulating the accumulation of IFT particles at the basal body (and possibly the loading of cargo to docked IFTs [37]). Ludington et al. [25] considered several different mathematical models of IFT regulation, based on the idea that cell signaling within the flagellum results in a length-dependent binding rate of IFT particles within the basal body and compared the models with experimental data on the length dependence of IFT. They applied two distinct ways of quantifying IFT. First, they used live imaging to measure the rate at which individual IFT particles were injected into flagella using GFP-tagged kinesin motors. Second, they fixed the cells and imaged IFT proteins that had accumulated at the basal bodies. The various deterministic models were then fitted with experimental curves obtained by averaging with respect to the flagellar population. Since several of the proposed models matched the experimentally obtained curves, the data were not sufficient to uniquely identify the most likely mechanism for IFT regulation. As noted by the authors, this was partly due to the large amount of scatter in the data; see Figure 6 of [25]. Such scatter could reflect heterogeneity in the population of flagella as well as various sources of intrinsic noise.

Further experimental evidence for stochasticity in IFT has been obtained by looking at statistical features of the time series of IFT injections [24]. The sequence of time intervals between consecutive injections exhibits transient periodicity, bursting activity, power-law dependencies, memory effects, and nonexponential interval statistics. Moreover, there are correlations between the frequency and size of injected IFT particles, with larger sizes (more IFT proteins within a particle) tending to occur less frequently. Based on these observations, Ludington et al. [24] suggested that the stochastic process of IFT injection exhibits avalanche-like behavior. The length-dependent binding of IFTs to the basal body then regulates the mean rate and size of IFT injections. Ludington et al. [24] also developed a computational model of the avalanche-like behavior, based on a cellular analog of a sandpile model. More specifically, they introduced a trafficking model for the passage of bound IFTs through the flagellar pore at the distal end of the basal body. The buildup of IFTs at the opening of the flagellum due to jamming effects then generated avalanche-like events, which were fitted to the experimental data. There are, however, a number of limitations of the computational model. First, the detailed mechanisms underlying the injection of IFTs into flagellar are currently unknown. Second, the computational model is analytically intractable. Third, the model assumes that the number of bound IFTs that drive the process is constant for a fixed length. With regard the third point, it is known that the number M of binding sites in the basal body is relatively small, $M \sim 100 - 1000$, so one would expect thermally driven fluctuations in the number of bound IFTs to introduce another level of stochasticity.

In this paper we follow a different approach to the stochastic modeling of IFT length control which is analytically more tractable and takes into account fluctuations in the number of bound IFTs. Rather than trying to develop a mechanistic model of IFT injections into the flagellum, we use a probabilistic model in the form of a doubly stochastic Poisson process (DSPP). DSPPs were first introduced by Cox [5] as a generalization of an inhomogeneous Poisson process, in which the time-dependent transition rate depends on a second, independent stochastic process. The general

theory of DSPPs was subsequently developed by Grandell [13]. Example applications include photon and electron detection [35, 32, 23], occurrences of credit events in finance [19], and neural coding [36, 34, 1, 18]. We use the theory of DSPPs to analyze how fluctuations in the binding/unbinding of IFTs at the basal body affect the injection of IFT particles into the flagellum, as well as flagellar length control. In order to develop the theory, we consider a much simpler model of IFT injections, namely, a Poisson process whose rate depends on the stochastic number of bound IFTs. Unlike a homogeneous Poisson process, the DSPP is not memoryless. We show that even this simple model captures some of the features of the experimental data on time series [24], such as nonexponential interevent interval statistics and time-dependent Fano factors. Moreover, the theory of DSPPs provides a mathematical framework for developing more complex stochastic models of IFT, following previous studies of neural spike trains [36] and photon detection [35, 23].

The organization of the paper is as follows. In section 2 we briefly describe the deterministic model of flagellar length control considered by Ludington et al. [25]. Our stochastic extension of this model is introduced in section 3, where we include fluctuations in IFT particle binding/unbinding within the basal body and model the injection of IFTs into the flagellum as a Poisson process. We then use the theory of DSPPs to analyze how IFT fluctuations depend on the number of binding sites. Finally, in section 4 we indicate how to construct more complex probabilistic models of IFT particle injection, highlighting an interesting link between event statistics in neural processes and the injection of IFTs.

2. Deterministic model. We begin by describing the deterministic model of flagellar length control introduced in [25]; see Figure 2.

2.1. Model of IFT flux. Consider a one-dimensional flagellum of length L with the basal body at $x = 0$ and the tip at $x = L$. Suppose that there are M binding sites for IFT particles in the basal body and the concentration of IFTs within the

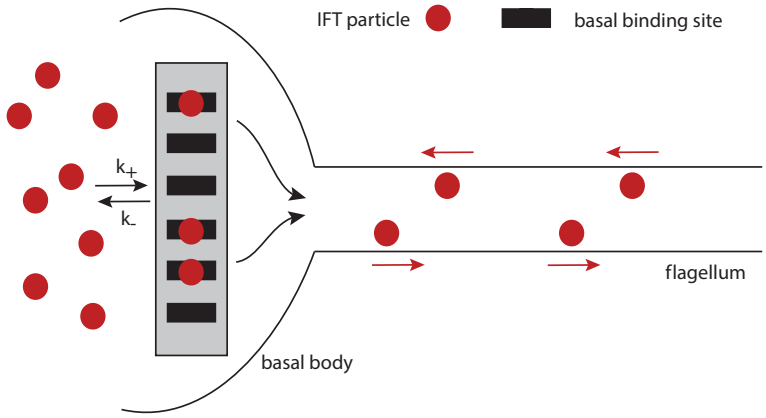

FIG. 2. *Schematic diagram of the basic model. IFT particles (filled circles) can undergo binding/unbinding reactions with M sites (filled rectangles) in the basal body at rates $k_\pm$. The number of bound IFTs determines the rate at which IFTs are injected into the flagellum. Once in the flagellum, IFTs are actively transported to the tip, where they deliver their cargo and are then transported back to the basal body along the lines shown in Figure* 1. *Some signaling mechanism within the flagellum (not shown) results in the binding rate k_+ being dependent on the flagellar length L, resulting in a length-dependent IFT flux regulation. For simplicity, all IFT particles are taken to be the same size.*

cytoplasm is B. Denote the binding and unbinding rates by k_+ and k_-, respectively. Assuming that M is sufficiently large, the kinetic equation for the number $m(t)$ of bound IFTs at time t is

$$\frac{dm}{dt} = k_+ B[M - m(t)] - k_- m(t), \tag{2.1}$$

which has the steady-state solution $m^* = k_+B/(k_+B + k_-)$. The number of binding sites M ranges from 10 to 1000, whereas fits with experimental data suggest that $\overline{k}_+B/k_- \sim 10\,\mu$m [24, 25]. Now suppose that there is some signaling mechanism within the flagellum such that the binding rate is a decreasing function of length L, and set $k_+ = \overline{k}_+C_0(L)$. We will give one example of such a signaling mechanism in section 2.2; see also [25]. Under the adiabatic approximation that the growth rate of the flagellum is much slower than the various kinetic processes, we can still treat m^* as a constant with

$$m^* = m^*(L) \equiv \frac{\overline{k}_+C_0(L)B}{\overline{k}_+C_0(L)B + k_-}M. \tag{2.2}$$

The rate of injection of IFTs into the flagellum is then taken to be $\lambda_0 = \eta m^*(L)$, which means that the influx is a monotonically decreasing function of L.

The critical flagellar length is determined by the balance between the influx and the length-independent rate of disassembly, along analogous lines to (1.1). That is, suppose each injected particle remains in the flagellum at time $T = 2L/v + \tau$ before being removed, where v is the harmonic mean of the anterograde and retrograde speeds of each IFT particle and τ is the time spent at the tip. We will take $\tau = 1$ s and $v = 2\,\mu$m/s. It follows that the steady-state number N^* of particles in the flagellum is

$$N^* = \lambda_0 T = \eta \frac{\overline{k}_+C_0(L)B}{\overline{k}_+C_0(L)B + k_-}M\,(2L/v + \tau)\,.$$

Hence, setting $N = N^*(L)$ in (1.1), we deduce that the critical length is determined by the intercept of the monotonically decreasing function $N^*(L)/L$ with a constant $\zeta = 2V/av$; see Figure 3.

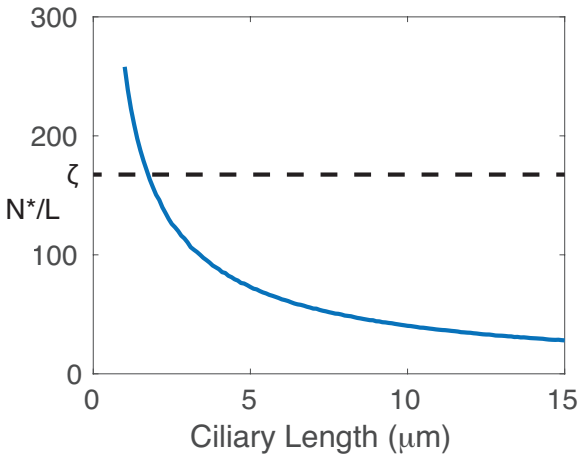

FIG. 3. *Plot showing relationship between average density of IFTs in flagellum and ciliary length and the existence of a unique stationary flagellum length for some constant* ζ.

2.2. RanGTP model of IFT flux regulation. The one remaining component of the model is the specification of the length-dependent function $C_0(L)$ of the IFT binding rate k_+. Ludington et al. [25] considered several different signaling mechanisms for generating this length dependence. For the sake of illustration, we will consider one of the models that fits particularly well with photobleaching data. It is a diffusion-based model of RanGTP concentration gradient formation. RanGTP is a small enzyme that is known to play an important role in regulating nuclear transport through the nuclear pore complex, and it is hypothesized that RanGTP plays an analogous role in regulating IFT particle influx. In particular, a decrease in RanGTP concentration at the basal body as cell length increases leads to a reduction in IFT particle influx.

Suppose that RanGTP is produced at a rate σ at the tip ($x = L$), resulting in a concentration gradient; see Figure 4. Assume that cytoplasmic RanGTP concentration is negligible and κ is the flow rate through the pore at $x = 0$. Then the RanGTP concentration per unit volume $C(x,t)$ evolves as

$$\frac{\partial C}{\partial t} = D\frac{\partial^2 C}{\partial x^2} - \gamma C, \quad x \in [0, L], \tag{2.3}$$

where γ is a degradation rate. The boundary conditions are

$$D\frac{\partial C}{\partial x} = \kappa C, \quad x = 0; \quad D\frac{\partial C}{\partial x} = \sigma, \quad x = L. \tag{2.4}$$

Integrating (2.3) with respect to x and using the boundary conditions gives

$$\frac{dR}{dt} = \sigma - \kappa C(0,t) - \gamma R,$$

where $R(t)$ is the total number of RanGTP molecules per unit area:

$$R(t) = \int_0^L C(x,t)dx. \tag{2.5}$$

If we assume that diffusion is fast so that the characteristic length $\sqrt{D/\gamma} \gg L$, then $C(x,t)$ is approximately uniform, and we can take $C(0,t) \approx R(t)/L$. Therefore,

$$\frac{dR}{dt} = \sigma - \kappa\frac{R}{L} - \gamma R. \tag{2.6}$$

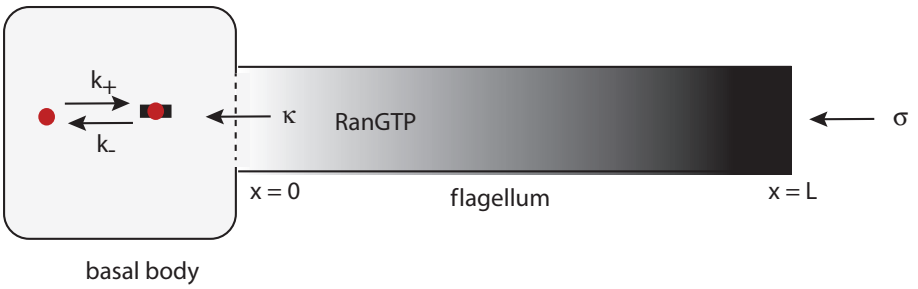

FIG. 4. *Schematic diagram of RanGTP concentration gradient model of IFT flux regulation. A source of RanGTP at the tip of the flagellum sets up a concentration gradient along the flagellum resulting in a length-dependent concentration of RanGTP in the basal body. This in turn regulates the binding rate of IFTs to sites in the basal body.*

Equation (2.6) has the steady-state solution

$$R = \frac{\sigma L}{\gamma L + \kappa},$$

so that the concentration at the basal pore is

$$C_0 = C_0(L) = \frac{\sigma}{\gamma L + \kappa}. \tag{2.7}$$

Typical values of the parameters are [25]

$$\sigma \sim 5 - 20/\text{s}, \quad \kappa \sim 5 - 25\,\mu\text{m/s}, \quad \gamma \sim 10 - 400/\text{s}.$$

Unless stated otherwise, we will take $\gamma/\sigma = 4$ and $\kappa/\sigma = 1\,\mu$m.

3. Stochastic model. There at least two possible sources of stochasticity that can be introduced into the above model; see Figure 2. First, rather than a constant injection rate λ_0 (for fixed length L), one can consider a stochastic model for the injection times of the particles. This was the approach taken by Ludington et al. [24], who considered a computational model to account for the avalanche-like behavior of IFT injections. In this paper, we will use a simpler probabilistic model based on a counting process in which we ignore variations in the size of injected particles. The second source of noise arises from the observation that the number of IFT binding sites in the basal body is relatively small; this will be the focus of our paper.

3.1. IFT injection as a Poisson process. We will refer to the injection of an IFT particle into the flagellum as an event. Let $N(t)$ be the number of events that have occurred in the interval $[0, t]$ such that

1. $N(0) = 0$;
2. $N(t) \in \{0, 1, 2, \ldots\}$ for all $t \geq 0$;
3. for $0 \leq s < t$, $N(t) - N(s)$ is the number of events in the interval $(s, t]$.

The random process $\{N(t), t \in [0, \infty)\}$ is said to be a *counting process* [6]. (Well-known examples of counting processes include the random arrival of customers at some service station resulting in the formation of a queue and the output spike trains of neurons.) A counting process can be characterized in terms of the occurrence or arrival times T_i of the ith event. This leads to two further definitions useful in characterizing counting processes. First, let $\{X(t), t \in [0, \infty)\}$ be a continuous-time stochastic process. We say that $X(t)$ has *independent increments* if, for all $0 \leq t_1 < t_2 \cdots < t_n$, the random variables $X(t_j) - X(t_{j-1})$, $j = 2, \ldots, n$, are independent. In the case of a counting process, this means that the numbers of arrivals in nonoverlapping time intervals are independent. Following on from this, $X(t)$ is said to have *stationary increments* if, for all $t_2 > t_1 \geq 0$ and all $r > 0$, the random variables $X(t_2) - X(t_1)$ and $X(t_2 + r) - X(t_1 + r)$ have the same distributions. In particular, a counting process has stationary increments if, for all $t_2 > t_1 \geq 0$, $N(t_2) - N(t_1)$ has the same distribution as $N(t_2 - t_1)$. In other words, the distribution of the number of events in an interval depends only on the length of the interval. Another useful quantity is the distribution of interarrival times $\tau_n = T_n - T_{n-1}$, where T_n is the nth arrival time, which can be defined iteratively according to

$$T_n = \inf\{t \geq 0 | N(t + T_{n-1}) = n\}, \quad T_0 = 0.$$

Suppose that the injection rate λ_0 is fixed. For simplicity, we will represent the injection of IFT particles by a homogeneous Poisson process for which $N(t)$ has

independent, stationary increments and the number n of arrivals in the interval $[0,t]$ has the Poisson distribution

$$P_n(t) = \frac{(\lambda_0 t)^n}{n!} \mathrm{e}^{-\lambda_0 t}. \tag{3.1}$$

It immediately follows that

$$\langle N(t) \rangle = \lambda_0 t, \quad \mathrm{Var}[N(t)] = \lambda_0 t.$$

Assuming that each IFT spends a time T in the flagellum (see section 2.1), the number of IFTs in the flagellum at time t is $\mathcal{N}(t) = N(t) - N(t-T)$. It is straightforward to show that $\mathcal{N}(t)$ for $t \geq T$ has the same distribution as $N(T)$, so that the mean and variance of the number of IFT particles within the flagellum is $\lambda_0 T$. In the case of a homogeneous Poisson process, the interarrival time probability density is an exponential, $\rho(\tau) = \lambda_0 \mathrm{e}^{-\lambda_0 \tau}$. It follows that the mean $\langle \tau \rangle = 1/\lambda_0$ and the variance is $\sigma_\tau^2 = 1/\lambda_0^2$.

3.2. Stochastic model of IFT docking at the basal body. The above analysis ignores temporal fluctuations in the number $m(t)$ of bound IFT particles, and the fact that when a particle is injected, it leaves a vacant binding site. For the moment, let us ignore the latter effect by assuming that the number of bound sites is much greater than one. This is a reasonable first approximation, given that experimentally one finds $M \sim 100 - 1000$ [25]. (Indeed, we will show in section 3.6 that this approximation only breaks down when $M \sim 1 - 100$.) The binding of IFTs is then independent of the Poisson process (but not vice versa). Let $Q_m(t)$ denote the probability that m out of M binding sites are bound by IFTs at time t. The corresponding master equation is

$$\begin{aligned} \frac{dQ(m,t)}{dt} &= k_+ B(M-m+1)Q(m-1,t) + k_-(m+1)Q(m+1,t) \\ &\quad - [k_+ B(M-m) + k_- m]Q(m,t) \end{aligned} \tag{3.2}$$

with $Q(-1,t) = Q(N+1,t) \equiv 0$. This can be rewritten in the form of the birth-death master equation

$$\begin{aligned} \frac{d}{dt}Q(m,t) &= \omega_+(m-1)Q(m-1,t) + \omega_-(m+1)Q(m+1,t) \\ &\quad - [\omega_+(m) + \omega_-(m)]Q(m,t) \end{aligned} \tag{3.3}$$

with transition rates

$$\omega_+(m) = (M-m)k_+ B, \quad \omega_-(m) = m k_-. \tag{3.4}$$

A standard calculation yields the steady-state solution $Q_s(m)$ of the master equation (3.3) [10, 4]. First, note that it satisfies $J(m) = J(m+1)$ with

$$J(m) = \omega_-(m)Q_s(m) - \omega_+(m-1)Q_s(m-1).$$

Using the fact that m is a nonnegative integer, that is, $Q_s(m) = 0$ for $m < 0$, it follows that $J(m) = 0$ for all m. Hence, by iteration,

$$Q_s(m) = Q_s(0) \prod_{k=1}^{m} \frac{\omega_+(k-1)}{\omega_-(k)} \tag{3.5}$$

with

$$Q_s(0) = \left(1 + \sum_{m=1}^{M} \prod_{k=1}^{m} \frac{\omega_+(k-1)}{\omega_-(k)}\right)^{-1}.$$

In the particular case of the transition rates (3.4), we have

$$Q_s(m) = Q_s(0) \left[\frac{k_+ B}{k_-}\right]^m \frac{M!}{m!(M-m)}. \tag{3.6}$$

After calculating $Q_s(0)$, we obtain the binomial distribution

$$Q_s(m) = \frac{(k_+B)^m k_-^{M-m}}{(k_+B+k_-)^M} \frac{M!}{m!(M-m)!} = (X^*)^m (1-X^*)^{M-m} \frac{M!}{m!(M-m)!}, \tag{3.7}$$

where $X^* = m^*/M$ with $m^* = k_+B/(k_+B+k_-)$. Using standard formulae for the moments of the binomial distribution, we find that, in the steady state, the mean number of bound IFTs at the basal body is $\langle m \rangle = MX^* = m^*$. Similarly, the steady-state variance is

$$\mathrm{Var}[m] = MX^*(1-X^*) \tag{3.8}$$

with $\sqrt{\mathrm{Var}[m]}/\langle m \rangle \sim 1/\sqrt{M}$. Hence, in the large M limit, we can simply treat the number of bound IFTs as a constant m. The injection of IFTs is then given by a homogeneous Poisson process with rate $\lambda_0 = \eta m^*$. However, since the total number of binding sites takes intermediate values, $M \sim 100 - 1000$ [25], we should really treat $m(t)$ as a stochastic variable evolving according to the birth-death master equation (3.2) and set $\lambda = \eta m(t)$. It follows that the process of IFT injection into the flagellum is described by the DSPP; see section 3.

In order to facilitate later calculations, we will carry out a system-size expansion of the master equation (3.2) for intermediate values of M [10, 4]. First, introduce the rescaled variable $x = m/M$ and corresponding transition rates $M\Omega_\pm(x) = \omega_\pm(Mx)$. Equation (3.2) can then be rewritten in the form

$$\begin{aligned}\frac{d\Pi(x,t)}{dt} = M[&\Omega_+(x-1/M)\Pi(x-1/M,t) + \Omega_-(x+1/M)\Pi(x+1/M,t) \\ &- (\Omega_+(x) + \Omega_-(x))\Pi(x,t)],\end{aligned} \tag{3.9}$$

where $\Pi(x,t) = Q(Mx,t)$. Treating x as a continuous variable and Taylor expanding terms on the right-hand side to second order in M^{-1} leads to the Fokker–Planck (FP) equation

$$\frac{\partial P(x,t)}{\partial t} = -\frac{\partial}{\partial x}\left[A(x)P(x,t)\right] + \frac{1}{2M}\sum_{k=1}^{M} \frac{\partial^2}{\partial x^2}\left[B(x)P(x,t)\right] \tag{3.10}$$

with

$$\begin{aligned} A(x) &= \Omega_+(x) - \Omega_-(x) = (1-x)k_+B - k_-x, \\ B(x) &= \Omega_+(x) + \Omega_-(x) = (1-x)k_+B + k_-x. \end{aligned}$$

The solution to the FP equation (3.10) determines the probability density function for a corresponding Itô stochastic process $X(t)$, which evolves according to the SDE

$$dX = A(X)dt + \sqrt{\frac{B(X)}{M}}dW(t). \tag{3.11}$$

Here $W(t)$ denotes an independent Wiener process such that

$$\langle W(t)\rangle = 0, \quad \langle W(t)W(s)\rangle = \min(t,s). \tag{3.12}$$

We now make the approximation $\lambda(t) = \eta M X(t)$. (Certain care must be taken, however, since there is a nonzero probability that $X(t)$ becomes negative. We will assume that this does not cause problems for sufficiently large M.)

3.3. IFT injection as a DSPP. Combining the two sources of noise outlined in sections 3.1 and 3.2, the homogeneous Poisson process becomes a DSPP. That is, $\{N(t), t \geq 0\}$ is a counting process with positive intensity $\lambda(X(t)) = \eta M X(t)$, which depends on a second independent stochastic process $\{X(t), t \geq 0\}$ with $X(t)$ the fraction of bound IFTs in the basal body. The latter evolves according to the SDE (3.11). For a given realization of the continuous stochastic process up to time t, $\{X(s), 0 \leq s < t\}$, the conditional probability distribution $P_n(t) \equiv \mathbb{P}[N(t) = n|\{X(s), 0 \leq s < t\}]$ satisfies the master equation

$$\frac{dP_n}{dt} = \lambda(X(t))[P_{n-1}(t) - P_n(t)], \tag{3.13}$$

which has the solution

$$P_n(t) = \frac{\Lambda(t)^n}{n!}\mathrm{e}^{-\Lambda(t)} \tag{3.14}$$

with

$$\Lambda(t) = \int_0^t \lambda(X(t'))dt'. \tag{3.15}$$

We now observe that the function $\Lambda(t)$ is itself stochastic with respect to different realizations $\{X(s), 0 \leq s < t\}$. Therefore, in order to determine the probability $\mathcal{P}_n(t)$ that the number of events in $[0,t)$ satisfies $N(t) = n$, it is necessary to average with respect to these different realizations. That is,

$$\begin{aligned}\mathcal{P}_n(t) &= \mathbb{E}_X\left[\mathbb{P}[N(t) = n|\{X(s), 0 \leq s < t\}]\right] \\ &= \mathbb{E}_X\left[\frac{1}{n!}\left(\int_0^t \lambda(X(s))ds\right)^n \exp\left(-\int_0^t \lambda(X(s))ds\right)\right],\end{aligned} \tag{3.16}$$

where $\mathbb{E}_X$ denotes expectations with respect to the stochastic process X. Introducing the characteristic function

$$G_{\Lambda(t)}(z) = \mathbb{E}_X\left[\mathrm{e}^{iz\Lambda(t)}\right], \tag{3.17}$$

it immediately follows that $\mathcal{P}_n(t)$ is related to the nth derivative of $G_{\Lambda(t)}(z)$:

$$\mathcal{P}_n(t) = \frac{(-i)^n}{n!}G_\Lambda^{(n)}(i).$$

Furthermore, we can express the characteristic function for $N(t)$ in terms of $G_{\Lambda(t)}$:

$$\begin{aligned}G_{N(t)}(z) \equiv \mathbb{E}\left[\mathrm{e}^{izN(t)}\right] &= \sum_{n\geq 0}\mathrm{e}^{izn}\mathcal{P}_n(t) = \sum_{n\geq 0}\mathbb{E}_X\left[\frac{1}{n!}\left(\mathrm{e}^{iz}\Lambda(t)\right)^n\mathrm{e}^{-\Lambda(t)}\right] \\ &= \mathbb{E}_X\left[\sum_{n\geq 0}\left(\frac{1}{n!}\left(\mathrm{e}^{iz}\Lambda(t)\right)^n\right)\mathrm{e}^{-\Lambda(t)}\right] = \mathbb{E}_X\left[\mathrm{e}^{\mathrm{e}^{iz}\Lambda(t)}\mathrm{e}^{-\Lambda(t)}\right] \\ &= G_{\Lambda(t)}(i - i\mathrm{e}^{iz}).\end{aligned}$$

In particular,

$$\mathbb{E}[N(t)] \equiv -i\frac{dG_{N(t)}(z)}{dz}\bigg|_{z=0} = -i\frac{dG_{\Lambda(t)}(i-ie^{iz})}{dz}\bigg|_{z=0} = \mathbb{E}_X[\Lambda(t)]. \tag{3.18}$$

In order to determine more general statistics of the DSPP, such as the covariance, we need to determine the joint characteristic function of a finite set of variables $\{N(t_1),\dots,N(t_m)\}$. This can be achieved using the notion of a characteristic functional [6, 2]; see the appendix. In particular, one obtains the following result for the covariance function (see (A.3)):

$$\begin{aligned} R_N(t_1,t_2) &= \mathbb{E}[N(t_1)N(t_2)] - \mathbb{E}[N(t_1)]\mathbb{E}[N(t_2)] \\ &= \mathbb{E}[\Lambda(t_1)\Lambda(t_2)] - \mathbb{E}[\Lambda(t_1)]\mathbb{E}[\Lambda(t_2)] + \mathbb{E}_X[\Lambda(t_1)]. \end{aligned} \tag{3.19}$$

Expressing $\Lambda(t)$ in terms of the intensity then gives

$$R_N(t_1,t_2) = \int_0^{t_1}\int_0^{t_2} R_\lambda(\tau,\tau')d\tau d\tau' + \int_0^{t_1}\mathbb{E}_X[\lambda(X(\tau))]d\tau,\ t_1 < t_2, \tag{3.20}$$

where

$$R_\lambda(\tau,\tau') = \mathbb{E}_X[\lambda(X(\tau))\lambda(X(\tau'))] - \mathbb{E}_X[\lambda(X(\tau))]\mathbb{E}_X[\lambda(X(\tau'))].$$

Another important quantity is the probability density $\rho(\tau)$ for the time τ between consecutive events, also known as the interevent interval density. Assuming that $X(t)$ is a stationary stochastic process, one finds that (see (A.7))

$$\rho(\tau) = \frac{1}{\mathbb{E}[\lambda]}\frac{d^2\mathcal{P}_0(\tau)}{d\tau^2} = \frac{1}{\mathbb{E}[\lambda]}\mathbb{E}\left[\left(\lambda(X(\tau))^2 - \lambda'(X(\tau))\right)\exp\left(-\int_0^\tau \lambda(X(s))ds\right)\right]. \tag{3.21}$$

3.4. Analysis of IFT fluctuations. The above analysis shows that determining the first-order and second-order statistics of the number $N(t)$ of injected IFT particles requires calculating the corresponding statistics of the stochastic intensity $\lambda(X(t)) = \eta M X(t)$, where $X(t)$ is the fraction of bound binding sites in the basal body. Thus, calculating the mean and covariance of the intensity reduces to determining these quantities for the solution of the SDE (3.11). We will assume that the Gaussian process is stationary so that $\langle X(t)\rangle = X^*$ with $X^* = m^*/M$ and

$$R_X(t_1,t_2) \equiv \langle [X(t_1) - \langle X(t_1)\rangle][X(t_2) - \langle X(t_2)\rangle]\rangle = \frac{X^*(1+\Theta)}{2M}e^{-\Gamma|t_2-t_1|},$$

where

$$\Gamma = k_+B + k_-, \quad \Theta = \frac{k_- - k_+B}{k_- + k_+B}.$$

Substituting these results into (3.18) and (3.20) gives

$$\mathbb{E}[N(t)] = \eta M\int_0^t \langle X(\tau)\rangle d\tau = \eta M X^* t = \lambda_0 t \tag{3.22}$$

and

$$\begin{aligned} R_N(t_1,t_2) &= \frac{\eta^2 M X^*(1+\Theta)}{2}\int_0^{t_1}\int_0^{t_2} e^{-\Gamma|\tau'-\tau|}d\tau d\tau' + \mathbb{E}[N(t_1)] \\ &= M\eta^2\frac{X^*(1+\Theta)}{2}\mathcal{A}(t_1,t_2) + \mathbb{E}[N(t_1)], \end{aligned}$$

where for $t_1 \leq t_2$,

$$\mathcal{A}(t_1,t_2) = \frac{2t_1}{\Gamma} - \frac{2}{\Gamma^2}\left[1-\mathrm{e}^{-\Gamma t_1}\right] + \frac{1}{\Gamma^2}\left[1-\mathrm{e}^{-\Gamma(t_2-t_1)} - \mathrm{e}^{-\Gamma t_1} + \mathrm{e}^{-\Gamma t_2}\right].$$

In particular, setting $t_1 = t_2 = t$ yields the variance

$$\mathrm{Var}[N(t)] = M\eta^2 \frac{X^*(1+\Theta)}{2}\left[\frac{2t}{\Gamma} - \frac{2}{\Gamma^2}\left[1-\mathrm{e}^{-\Gamma t}\right]\right] + \mathbb{E}[N(t)]. \tag{3.23}$$

Note that for all $t > 0$, we have

$$\mathrm{Var}[N(t)] > \mathbb{E}[N(t)].$$

The latter is a basic property of DSPPs, namely, that the variance is greater than a Poisson process with intensity given by the mean of the stochastic intensity—a feature known as *overdispersion*. In particular, for sufficiently large t,

$$\mathrm{Var}[N(t)] \sim \lambda_1 t, \quad \lambda_1 = \lambda_0\left(1+\eta\frac{1+\Theta}{\Gamma}\right). \tag{3.24}$$

We also note that in the limit of fast binding/unbinding, $\Gamma \to \infty$, the DSPP reduces to a homogeneous Poisson process with $\mathrm{Var}[N(t)] \to \mathbb{E}[N(t)]$. This reflects the fact that the state of each binding site becomes essentially delta-correlated, so the sum of the Poisson processes emerging from each binding site can be viewed as a marked Poisson process where each potential transmission of an IFT particle is rejected (independently) if the binding site was vacant at that time. Hence, the non-Poisson character comes entirely from the temporal correlations (finite Γ) of the states of the binding sites.

The analysis of a Gaussian-driven DSPP is well known within the theory of point processes [6]. However, our main concern is using this analysis to investigate how fluctuations in IFT depend on the number of binding sites M and the flagellar length L. The latter dependence is obtained by including the regulatory feedback described in section 2, whereby the binding rate takes the form $k_+ = \overline{k}_+ C_0(L)$ with $C_0(L)$ given by (2.7).

In Figure 5 we show histograms for the number $N(T)$ of IFTs injected into the flagellum during the time interval $[0,T]$ for $M = 200$ and $M = 20$. We obtain

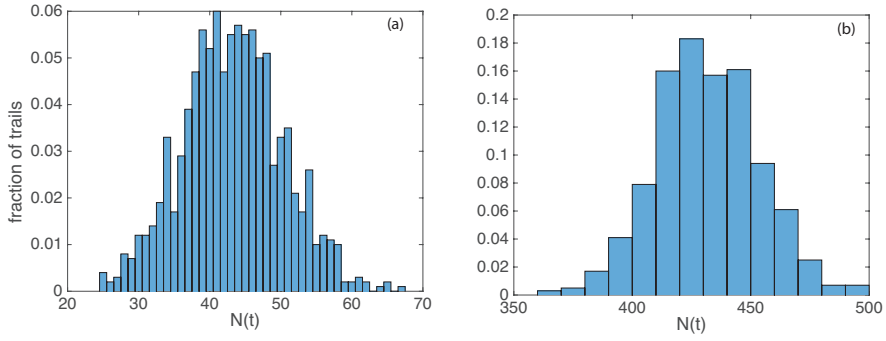

FIG. 5. *Histogram depicting $N(T)$ for $L = 10\,\mu$m over 1000 trials.* (a) $M = 20$ *with* $\langle N(T)\rangle \approx 43.5$ *and* $Var[N(T)] \approx 50.6$. (b) $M = 200$ *with* $\langle N(T)\rangle \approx 433$ *and* $Var[N(T)] \approx 436$. *Both histograms depict overdispersion, but it is more siginifcant for small M. Other parameter values are* $B\overline{k}_+/k_- = 10$, $\eta = 1/$s, $\kappa/\sigma = 1\,\mu$m, $\gamma/\sigma = 4$, $\tau = 1$ s, *and* $v = 2\,\mu$m/s.

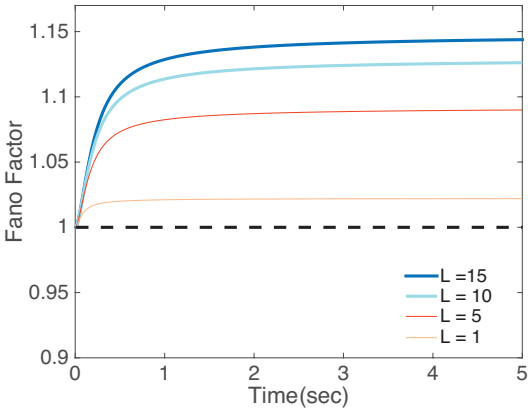

FIG. 6. *Deviation of Fano factor from Poisson case for different flagellar lengths. Other parameters are as in Figure* 5.

the results using a thinning algorithm; see section 3.5. One finds that both cases exhibit overdispersion. It can also be seen that the histogram in the small M case is considerably noisier than the histogram in the large M case, which is relatively smooth. Our results suggest that there is an M-dependent contribution to fluctuations in the number $N(T)$ of IFT particles within the flagellum and that there is a deviation from a homogeneous Poisson process.

A useful quantity for characterizing fluctuations of a counting process is the Fano factor (F_N), which is the ratio of the variance over the mean. It is used extensively in the study of neural spike trains and gene networks. From (3.22) and (3.23), we have

$$F_N(t) := \frac{\mathrm{Var}[N(t)]}{\mathbb{E}[N(t)]} = 1 + \left(\frac{\lambda_1}{\lambda_0} - 1\right)\left(1 - \frac{1 - \mathrm{e}^{-\Gamma t}}{\Gamma t}\right). \tag{3.25}$$

It is clear that $F_N(t)$ is a monotonically increasing function of time with $F_N(0^+) = 1$ and $F_N(t) \to \lambda_1/\lambda_0 > 1$ as $t \to \infty$. Moreover, it is independent of M but depends on flagellar length L due to the regulatory feedback, as shown in Figure 6. Recall that a homogeneous Poisson process has a Fano factor of one. Hence, at larger times our model exhibits non–Poisson-like behavior with a Fano factor greater than one, which is consistent with bursting. This is also consistent with what is observed experimentally; see Figure S1 of [24]. One discrepancy between our model and the experimental data is that at small times the experimentally determined Fano factor dips below one, indicative of behavior more regular than Poisson (e.g., transient periodicity). However, one can obtain such behavior by introducing some form of refractory effect.

A direct way to introduce a refractory period τ_r into the IFT model is to impose the additional constraint that if an IFT particle is injected at time T_n, then no subsequent injection events can occur in the interval $[T_n, T_n + \tau_r]$. Although it is difficult to obtain analytical results in this case, numerical simulations show that this modification yields an interevent interval density $\rho(\tau)$ with a peak and a Fano factor that lies below one at small times. This is illustrated in Figure 7. Roughly speaking, refractoriness arises from the process whereby bound IFT particles traffic through the basal body before being injected into the flagellum.

Let us now turn to the time series of events generated by the DSPP. In the case of a Gaussian DSPP, we have

$$\mathcal{P}_0(t) = \mathrm{e}^{-\lambda_0 t + A(t)},$$

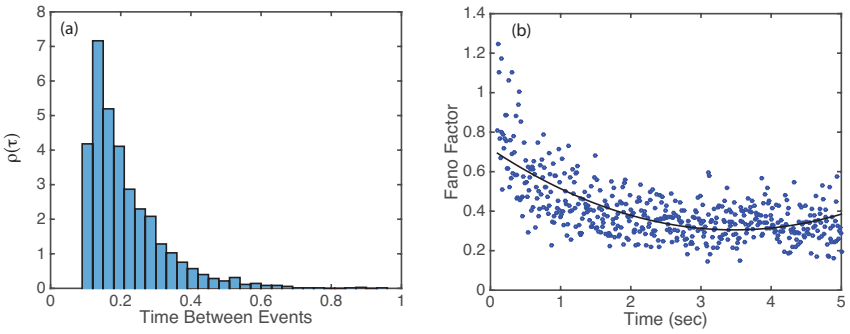

FIG. 7. *Effects of a refractory period* τ_r. (a) *Histogram of interevent interval density* $\rho(\tau)$ *as a function of time* τ. (b) *Plot of Fano factor at small times. Dots represent data points and the black curve is the mean Fano factor. We take* $L = 10\,\mu m$, $\tau_r = 0.1$ *sec, and the other parameters are as in Figure* 8.

where $\mathbb{E}_X[\Lambda(t)] = \lambda_0 t$ and

$$A(t) = \mathrm{Var}[\Lambda(t)]/2 = M\eta^2 \frac{X^*(1+\Theta)}{4}\left[\frac{2t}{\Gamma} - \frac{2}{\Gamma^2}\left[1 - \mathrm{e}^{-\Gamma t}\right]\right].$$

Equation (3.21) implies that the interevent interval density is

$$\rho(\tau) = \lambda_0 \left[\left(1 - \frac{1}{\lambda_0}\frac{dA(t)}{dt}\right)^2 + \frac{1}{\lambda_0^2}\frac{d^2A(t)}{dt^2}\right]\mathcal{P}_0(t).$$

Plots of $\rho(\tau)$ and sample event time series for various M and L are shown in Figure 8. This establishes that $\rho(\tau)$ differs from the exponential density of a homogeneous Poisson process, and this difference increases as M decreases and L increases. The corresponding time series become more bursty. The increase of the non–Poisson-like behavior with L reflects the fact that the binding rate decreases with L due to the regulatory feedback.

3.5. Numerical methods. We simulate the DSPP using a thinning algorithm [21] as follows. Consider a nonhomogeneous Poisson process on the time interval $[0, T]$ with rate function $\lambda(t)$, and assume there exists a constant λ^* such that $\lambda^* \geq \lambda(t)$ on $[0, T]$. To simulate the nonhomogeneous Poisson process, first consider the *homogeneous* Poisson process with rate λ^*. We now generate a sequence of times $T_1, T_2, \ldots, T_m$ for $m \in \mathbb{N}$ with $0 < T_1 < T_2 < \ldots < T_m \leq T$, with T_i, $i = 1, \ldots, m$ corresponding to the time of the ith injection of IFTs docked at the basal body into the flagellum. To obtain the sequence of injection times for the nonhomogeneous Poisson process with rate $\lambda(t)$, we accept each T_i generated from the homogeneous Poisson process with probability $\lambda(T_i)/\lambda^*$. The resulting sequence of injection times corresponds to the nonhomogeneous Poisson process with rate function $\lambda(t)$. For a rigorous proof of this, see [21]. For our particular model, we employ the thinning algorithm by utilizing the following procedure:

- Generate a stochastic trajectory $X(t)$ according to (3.11) on the interval $[0, T]$.
- Compute $\lambda(X(t)) = \eta M X(t)$, and let $\lambda^* = \max(\lambda(X(t)))$.
- Generate a sequence of times $T_1, T_2, \ldots, T_m$ with $0 < T_1 < T_2 < \ldots < T_m \leq T$ from an exponential distribution with parameter λ^*.

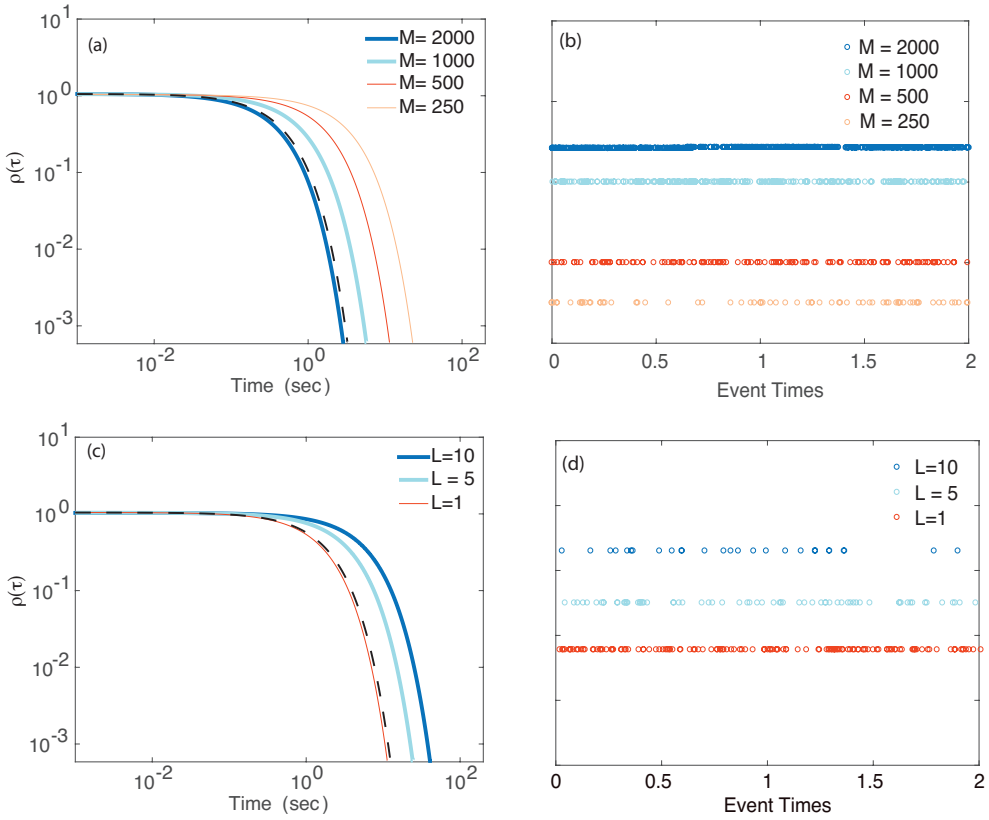

FIG. 8. *Plots of $\rho(t)$ and the corresponding time series for assorted values of M and L.* (a, b) $L = 10\,\mu$m, (c, d) $M = 100$. *Other parameter values are* $B\overline{k}_+/k_- = 10$, $\eta = 1/$s, $\kappa/\sigma = 1\,\mu$m, $\gamma/\sigma = 4$, $\tau = 1s$, *and* $v = 2\,\mu$m/s. *Dashed line shows exponential density for a homogeneous Poisson process.*

- For each T_i, $i = 1, .., m$, generate a random number U_i distributed uniformly on the interval $[0, 1]$.
- If $\lambda(X(T_i))/\lambda^* \geq U_i$, accept T_i as a firing time generated by the nonhomogeneous Poisson process with rate $\lambda(X(t))$. Otherwise, do not include T_i as a firing time generated by the nonhomogeneous Poisson process.

3.6. Effects of very small M. Our formulation of flagellar length control as a DSPP relies on the assumption that the number M of binding sites within the basal body is sufficiently large so that the binding process is independent of the Poisson process (but not vice versa). On the other hand, when $M \sim 1 - 100$, we have to consider the joint stochastic process that simultaneously keeps track of the number of bound IFTs $M(t)$ and the number $N(t)$ particles injected into the flagellum. Assuming that the latter is still given by a Poisson process, the master equation for the joint probability distribution $P_{m,n}(t) = \mathbb{P}(M(t) = m, N(t) = n|M(0) = m_0, N(t) = 0)$ is

(3.26)
$$\frac{dP_{m,n}}{dt} = k_+B(M-m+1)P_{m-1,n}(t) + k_-(m+1)P_{m+1,n}(t) \\ -[k_+B(M-m) + k_-m]P_{m,n}(t) + \eta(m+1)P_{m+1,n-1}(t) - \eta m P_{m,n}(t).$$

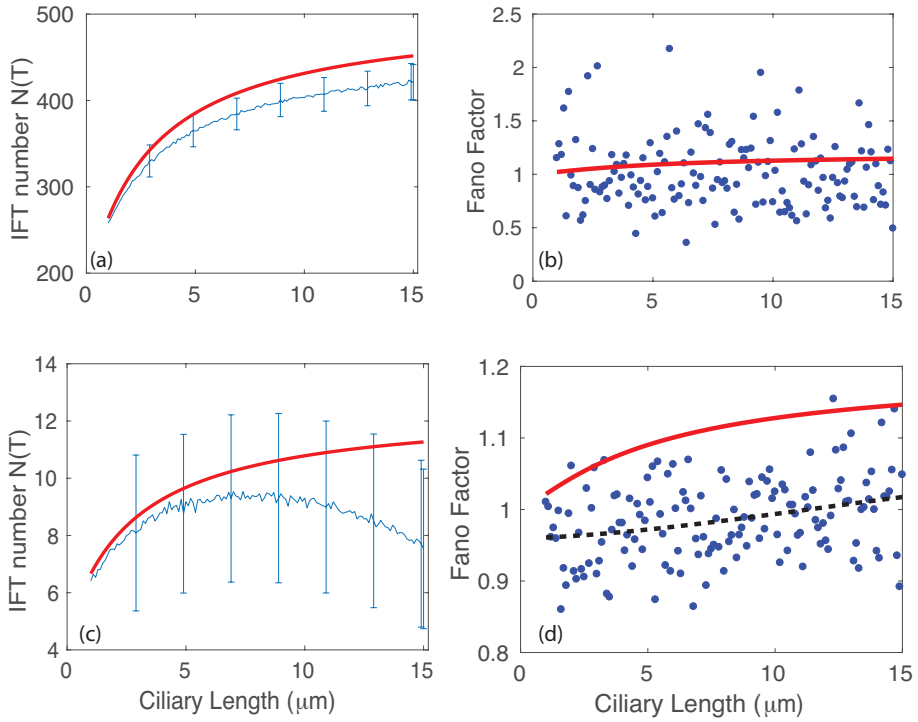

FIG. 9. *Simulation results of discrete stochastic process with corresponding master equation* (3.26) *averaged over* 200 *trials.* (a, c) *Plots of number of injected IFT particles* $N(T)$ *in interval* $[0,T]$ *for* $M=200$ *and* $M=5$, *respectively.* (b, d) *Corresponding plots of the Fano factor* $F(T)$. *The dots and thin (blue) curves are simulation results. Analytical curve are shown by thick (red) curves. The dashed curve in* (d) *is the mean Fano factor obtained from the numerical data. Other parameter values are* $B\bar{k}_+/k_- = 10$, $\eta = 1/\text{s}$, $\kappa/\sigma = 1\,\mu\text{m}$, $\gamma/\sigma = 4$, $\tau = 1\,\text{s}$, *and* $v = 2\,\mu\text{m/s}$.

The mean number of particles injected in the interval $[0,t]$ is

$$\langle N(t)\rangle = \sum_{m=0}^{M}\sum_{n\geq 0} nP_{m,n}(t). \tag{3.27}$$

Unfortunately, is not possible to obtain exact analytical solutions to the full master equation, so we will investigate the effects of very small M using computer simulations.

For numerical simulations of the full stochastic system given by (3.26), we use a continuous-time Monte Carlo algorithm based on the Gillespie algorithm [11]. Plots of $\langle N(T)\rangle$ and the Fano factor $F(T)$ versus ciliary length are shown in Figure 9. In the intermediate M regime (Figure 9(a) and 9(b)), we find that numerical results obtained from the chemical master equation (3.26) are in good agreement with the analytical results from (3.22) and (3.23). Figure 9(c) and 9(d) depicts the mean and Fano factor of injected IFTs versus ciliary length in the small M regime. It can be seen that the numerical results deviate significantly from the analytical results, consistent with the breakdown of the system-size expansion in this regime and the emerging dependence of the stochastic binding process on IFT particle injections. Note in particular that the mean number of IFT particles $\langle N(T)\rangle$ decreases for large L. Interestingly, we find that the density $\rho(\tau)$ of interevent time intervals does not significantly change its qualitative behavior in the small M regime; see Figure 10

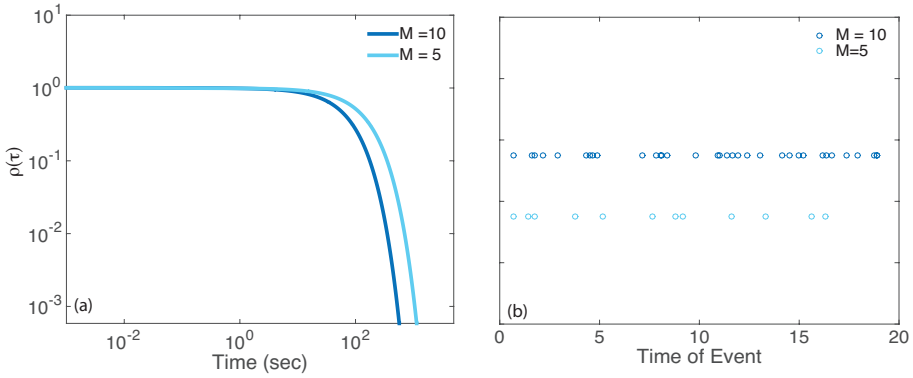

FIG. 10. *Simulation results of* (3.26). (a) $\rho(t)$ *for small* M *and* $L = 10\,\mu$m. (b) *Time series for injection events in the small* M *case for* $L = 10\,\mu$m. *Other parameter values are as in Figure* 8.

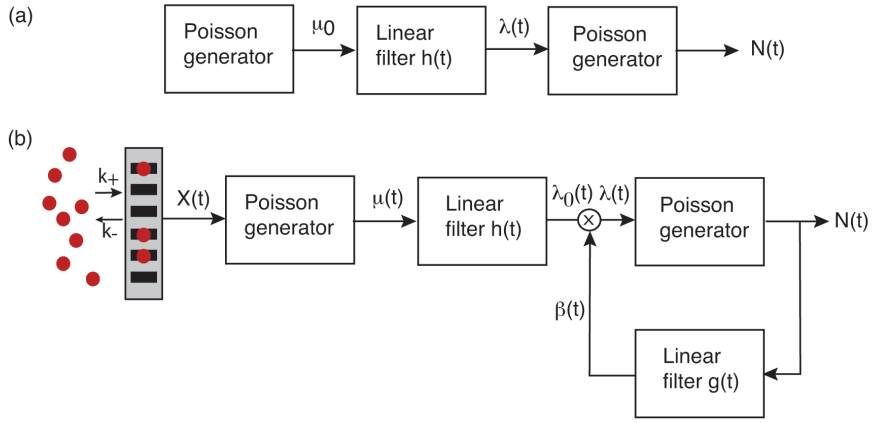

FIG. 11. *Stochastic representation of an SNDP.* (a) *Standard SNDP with no feedback.* (b) *Self-excited SNDP with the additional feature that the rate of the first Poisson process is also stochastic due to the binding/unbinding of IFT particles.*

4. Extensions of the stochastic model. So far we have modeled the import of IFT particles into the flagellum as a counting process $\{N(t), t \geq 0\}$ consisting of two components: the stochastic binding and unbinding of IFT particles at the basal body and the stochastic release of IFT particles into the flagellum itself. For simplicity, we have taken the latter to be a Poisson process. However, this cannot capture the full complexity of the time series of release events observed experimentally [24], such as nonmonotonic time-dependent Fano factors, peaks in the interevent interval density $\rho(\tau)$, and power-law dependencies. All of these latter features are also found in another application domain, namely, neural spike trains [36, 34]. A common modeling strategy in these cases is to consider a shot-noise–driven DSPP, which we will denote by SNDP, and to introduce some form of refractoriness. In this section we indicate how such models could be adapted to IFT. One particular application of such models would be to investigate to what extent details regarding the time series affect flagellar length regulation, particularly given that the latter occurs on longer time scales.

A schematic diagram of a basic SNDP is shown in Figure 11(a). It consists of two Poisson processes separated by a linear filter. The first Poisson process generates

events at a constant rate μ_0 resulting in a sequence of event times t_k, $k = 0, 1, \ldots$. These event times are fed into the linear filter with kernel function $h_1(t)$, $h_1(t) = 0$ for $t < 0$, resulting in the filtered Poisson process or shot noise

$$\lambda(t) = \sum_{k\geq 0} h_1(t - t_k). \tag{4.1}$$

Phenomenologically speaking, h could represent the effects of IFT particle trafficking within the basal body. Finally, $\lambda(t)$ is taken to be the stochastic rate of the second Poisson process, resulting in an SNDP. A typical choice for $h(t)$ is the exponential filter $h(t) = h_0 \mathrm{e}^{-t/\tau_h}$ for $t > 0$. However, in cases where the statistics of a counting process display power-law dependencies over a significant range of times (fractal behavior), it is more appropriate to consider fractal shot noise for which $h(t) = h_0 t^{-\alpha}$ for some $\alpha > 0$ [23, 36]. Another modification of the basic SDNP is to add a feedback loop as shown in Figure 11(b), which represents a form of self-excitation [35]. Whenever an event occurs, this feedback modifies the rate of succeeding events by a multiplicative factor $\beta(t)$ generated by a second filter function $g(t)$ such that

$$\lambda(t) = \beta(t)\lambda_0(t) = \beta(t) \sum_{k\geq 0} h(t - t_k), \quad \beta(t) \sum_{l\geq 0} g(t - T_l), \tag{4.2}$$

where T_l are the event times of the second Poisson process. In the case of neural spike trains, a typical choice of the filter g is $g(t) = 1 - \mathrm{e}^{-t/\tau_d}$ for $t > 0$ and zero otherwise. This represents the effects of relative refractoriness, whereby when a neuron fires, its likelihood of firing another spike in quick succession is reduced. In the case of IFT, an analog of refractoriness could be the time new material needs to take to pass through the basal body so that it is ready for injection into the flagellum [24].

There are additional complicating factors in applying SNDPs to IFT. First, the rate of the first Poisson process is itself stochastic since it is driven by the random process of IFTs binding to the basal body. Hence, the full model consists of a pair of DSPPs connected in series; see Figure 11(b). Second, in contrast to standard neural spike trains, for which the size of each event (firing of a single action potential) is identical, the size of IFT injection events varies and is correlated with the frequency of such events. This raises the mathematical issue of how to incorporate event size into the counting process. One approach would be to treat the second Poisson process as a marked Poisson process [7]. The latter is defined as follows: Let $N(t)$ be a Poisson process with event times $\{T_n, n > 0\}$. Given some space $\mathcal{M}$, if a random mark $m_n \in \mathcal{M}$ is attached to each event $N(t) = n$, then $X = \{(T_{N(t)}, m_{N(t)}), t > 0\}$ is said to be a marked Poisson process.

The simplest model for marks is to take them to be independent and identically distributed random variables that are independent of the event times T_n. The next level of complexity is to assume that the marks are statistically correlated but still independent of the event times. Yet another level of complexity is to assume that there is a correlation between the event times and the marks. For example, suppose that $\lambda(t)$ denotes the rate of the second Poisson process and

$$m_n = a + b\lambda(T_n) + X_n, \tag{4.3}$$

where a, b are constants and X_n is some additional independent random variable (which could be zero). If $b < 0$, then the size of a mark will be larger when the rate of events is smaller. If we interpret m_n as the size of the nth injected IFT particle, then this correlation would be consistent with what is observed experimentally.

5. Discussion. In this paper we presented a model of flagellar length control based on a DSPP in which we assumed that the injection times of IFT into a flagellum from the basal body are given by an inhomogeneous Poisson process whose rate is based on the number of IFTs bound at the basal body. The number of IFTs bound to the basal body in turn evolves according to a stochastic birth-death process, hence rendering the Poisson rate of injection times of IFT into the flagellum stochastic. We used the theory of DSPPs to analyze the effects of fluctuations on IFT and showed how our model captures some of the qualitative features of the experimental time series data on the import of IFT particles into flagella, in particular, the nonexponential interevent interval statistics and time-dependent Fano factors. We also established that reducing the number M of available binding sites on the basal body can significantly affect length regulation.

To what extent could the M dependence predicted by the stochastic model be investigated experimentally? One possibility would be to pharmacologically add an agonist that can bind to sites on the basal body without interfering with other components of the IFT process (assuming such an agonist can be found). One would then expect the effective number of free binding sites M_{eff} to decrease as the concentration of agonist increases, thus increasing the level of fluctuations.

One of the main goals of this paper was to develop the mathematical link between the length-dependent regulation of IFT and counting processes. In particular, we noted that many of the features of the time series of IFT injection events occur in neural spike trains. This motivated us to model IFT dynamics within the basal body and subsequent release of IFTs into the flagellum as a DSPP, analogous to the use of DSPPs to model neural processing within the soma leading to the firing of an action potential. A major challenge in future work will be to develop more sophisticated probabilistic models of IFT that better fit the data. One approach, which is inspired by neural modeling, is to consider the serially linked DSPPs shown schematically in Figure 11(b). Although it should be possible to analyze such a model, another issue is determining the most appropriate choice of the filters h and g, either by data fitting or by using information regarding the physical structure of the basal body. Finally, as highlighted at the end of section 4, we need to explore ways to take into account variations in the size of events and how they correlate with the frequency of events using, for example, the theory of marked point processes.

There are a number of other possible extensions of our work. First, we have modeled the ballistic motion of the IFTs along the flagellum deterministically, whereas in reality the motion is more random due to switching between different motile states [3]. It also possible that the amount of time τ spent at the tip of the flagellum by each IFT is a random variable. Both of these features would add further levels of stochasticity. Another generalization would be to consider cases where the number of particles available to bind to a basal body (in our model this is represented by the concentration B) is finite and is divided between two or more flagella that are competing for growth [12, 30]. Finally, it would be interesting to apply DSPP models to other examples of intracellular transport. For example, we recently developed a model that describes an axonal length sensing mechanism based on motor transport [15]. In this model, injection rates of motors were taken to be deterministic rather than dictated by a Poisson process.

Appendix A.

In this appendix we gather a few basic results in the theory of point processes and DSPPs. See [6, 7] for more details.

Correlations of a DSPP. Let $\{N(t), t \geq 0\}$ denote a DSPP. Introduce the characteristic functional [6, 2]

$$\Phi_N[v] \equiv \mathbb{E}\left[\exp\left(i\int_0^T v(\sigma)dN(\sigma)\right)\right] \tag{A.1}$$

for fixed T, where v is a real-valued function and the integral is a counting integral,

$$\int_0^T v(\sigma)dN(\sigma) = \sum_{i=1}^{N(T)} v(\omega_i),$$

with ω_i denoting the occurrence times of the DSPP. Expectation is taken with respect to both stochastic processes $N(t), X(t)$. In order to evaluate the characteristic functional, we first condition on a particular realization $\{x(t), 0 \leq t \leq T\}$ of the stochastic process $X(t)$ over the time interval $[0, T]$. We write the corresponding conditioned characteristic functional as

$$\Phi_N[v|x] \sim \mathbb{E}\left\{\exp\left(i\sum_{k=1}^{M} v(\sigma_k)\Delta N(\sigma_k)\right)\right\}.$$

Time has been discretized time into M intervals of size $\Delta\sigma$, and expectation is taken with respect to the inhomogeneous Poisson process with intensity $\lambda(t) = \lambda(x(t))$. (We are assuming that the limit $M \to \infty, \Delta\sigma \to 0$ with $M\Delta\sigma = T$ is well defined.) It follows that

$$\begin{aligned}\Phi_N[v|x] &\sim \prod_{k=1}^{M}\left[(1-\lambda(\sigma_k)\Delta\sigma) + \lambda(\sigma_k)\Delta\sigma\exp\left(iv(\sigma_k)\right)\right]\\ &\sim \prod_{k=1}^{M}\exp\left(\left[\mathrm{e}^{iv(\sigma_k)}-1\right]\lambda(\sigma_k)\Delta\sigma\right)\\ &\sim \exp\left(\sum_{k=1}^{M}\left[\mathrm{e}^{iv(\sigma_k)}-1\right]\lambda(\sigma_k)\Delta\sigma\right).\end{aligned}$$

If we now retake the continuum limit, we see that

$$\Phi_N[v|x] = \exp\left(\int_0^T\left[\mathrm{e}^{iv(\sigma)}-1\right]\lambda(\sigma)d\sigma\right).$$

Finally, taking expectation with respect to the stochastic process $X(t)$ yields

$$\Phi_N[v] = \mathbb{E}_X\left\{\exp\left(\int_0^T\left[\mathrm{e}^{iv(\sigma)}-1\right]\lambda(\sigma)d\sigma\right)\right\}. \tag{A.2}$$

Let $v(\sigma)$ be the following piecewise function [2]:

$$v(\sigma) = \begin{cases} \sum_{i=1}^{m}\alpha_i; & 0 \leq \sigma < t_1\\ \sum_{i=2}^{m}\alpha_i; & t_1 \leq \sigma < t_2\\ \vdots & \vdots\\ \alpha_m; & t_{m-1} \leq \sigma < t_m\\ 0; & t_m \leq \sigma < T,\end{cases}$$

where $0 < t_1 < t_2 < \cdots < t_m < T$. From (A.1), the corresponding characteristic functional is

$$\begin{aligned}\Phi_N[v] &= \mathbb{E}\left\{\exp[i(\alpha_1+\cdots+\alpha_m)N(t_1) + i(\alpha_2+\cdots+\alpha_m)(N(t_2)-N(t_1))\right.\\ &\qquad \left.+\cdots+i\alpha_m(N(t_m)-N(t_{m-1}))]\right\}\\ &= \mathbb{E}\left\{\exp[i(\alpha_1 N(t_1)+\cdots+\alpha_m N(t_m)]\right\} = G_{N(t_1),\ldots,N(t_m)}(\alpha_1,\ldots,\alpha_m),\end{aligned}$$

where $G_{N(t_1),\ldots,N(t_m)}$ is the joint characteristic function of $(N(t_1),\ldots,N(t_m))$. On the other hand, from (A.2) we have

$$\begin{aligned}\Phi_N[v] &= \mathbb{E}_X\left\{\exp\left[\left(\mathrm{e}^{i(\alpha_1+\cdots+\alpha_m)}-1\right)\int_0^{t_1}\lambda(\sigma)d\sigma+\cdots+\left(\mathrm{e}^{i\alpha_m}-1\right)\int_{t_{m-1}}^{t_m}\lambda(\sigma)d\sigma\right]\right\}\\ &= \mathbb{E}_X\left\{\exp\left[\left(\mathrm{e}^{i(\alpha_1+\cdots+\alpha_m)}-\mathrm{e}^{i(\alpha_2+\cdots+\alpha_m)}\right)\Lambda(t_1)+\cdots+\left(\mathrm{e}^{i\alpha_m}-1\right)\Lambda(t_m)\right]\right\}\\ &= G_{\Lambda(t_1),\ldots,\Lambda(t_m)}\left(-i\mathrm{e}^{i(\alpha_1+\cdots+\alpha_m)}+i\mathrm{e}^{i(\alpha_2+\cdots+\alpha_m)},\ldots,i-i\mathrm{e}^{i\alpha_m}\right),\end{aligned}$$

where $G_{\Lambda(t_1),\ldots,\Lambda(t_m)}$ is the joint characteristic function of $(\Lambda(t_1),\ldots,\Lambda(t_m))$. For the sake of illustration, consider the case $m=2$ and the covariance function

$$\begin{aligned}R_N(t_1,t_2) &= \mathbb{E}[N(t_1)N(t_2)] - \mathbb{E}[N(t_1)]\mathbb{E}[N(t_2)]\\ &= -\frac{\partial^2 G_{N(t_1),N(t_2)}(\alpha_1,\alpha_2)}{\partial\alpha_1\partial\alpha_2}\bigg|_{\alpha_1=\alpha_2=0} - \mathbb{E}_X[\Lambda(t_1)]\mathbb{E}_X[\Lambda(t_2)]\\ &= -\frac{\partial^2 G_{\Lambda(t_1),\Lambda(t_2)}(-i\mathrm{e}^{i(\alpha_1+\alpha_2)}+i\mathrm{e}^{i\alpha_2}, i-i\mathrm{e}^{i\alpha_2})}{\partial\alpha_1\partial\alpha_2}\bigg|_{\alpha_1=\alpha_2=0}\\ &\qquad -\mathbb{E}_X[\Lambda(t_1)]\mathbb{E}_X[\Lambda(t_2)]\\ &= \mathbb{E}_X[\Lambda(t_1)\Lambda(t_2)] + \mathbb{E}_X[\Lambda(t_1)] - \mathbb{E}_X[\Lambda(t_1)]\mathbb{E}_X[\Lambda(t_2)]\\ &= R_\Lambda(t_1,t_2) + \mathbb{E}_X[\Lambda(t_1)]. \qquad \text{(A.3)}\end{aligned}$$

Interevent interval density. Consider a counting process with stationary increments. Let $N(t_1,t_2)$ denote the number of events in the interval $(t_1,t_2]$ so that $N(t) = N(0,t)$. Introduce the survivor function for the time X between consecutive events:

$$F_X(x) = \mathbb{P}[X > x] = \lim_{\delta\to 0^+}\mathbb{P}[N(0,x)=0 | N(-\delta,0)>0]. \qquad \text{(A.4)}$$

This is the probability that following an event at $t=0^-$, there is not another event up to time $t=x$. By stationarity,

$$\begin{aligned}\mathbb{P}[\{N(0,x)=0\}\cup\{N(-\delta,0)>0\}] &= \mathbb{P}[N(0,x)=0] - \mathbb{P}[N(-\delta,x)=0]\\ &= \mathbb{P}[N(x)=0] - \mathbb{P}[N(x+\delta)=0].\end{aligned}$$

Hence,

$$\mathbb{P}[N(0,x)=0|N(-\delta,0)>0]\mathbb{P}[N(\delta)>0] = \mathbb{P}[N(x)=0] - \mathbb{P}[N(x+\delta)=0].$$

Dividing both sides by δ and taking the limit $\delta\to 0$ with

$$\nu = \lim_{\delta\to 0^+}\mathbb{P}[N(\delta)>0]$$

(assuming ν exists) establishes that

$$F_X(x) = -\frac{1}{\nu}\frac{dP_0(x)}{dx}, \tag{A.5}$$

where $P_n(x) = \mathbb{P}[N(x) = k]$, $k = 0, 1, \ldots$. Finally, the interevent interval density is

$$\rho(\tau) = -\left.\frac{dF_X(x)}{dx}\right|_{x=\tau} = \frac{1}{\nu}\frac{d^2P_0(\tau)}{d\tau^2}. \tag{A.6}$$

In the case of a Poisson process, ν can be identified with the Poisson rate λ_0, whereas in the case of a DSPP, $\nu = \mathbb{E}[\lambda]$ and $P_0(\tau) \to \mathcal{P}_0(\tau) = \mathbb{E}[P_0(\tau)]$:

$$\rho(\tau) = \frac{1}{\mathbb{E}[\lambda]}\frac{d^2}{d\tau^2}\mathbb{E}\left[\exp\left(-\int_0^\tau \lambda(s)ds\right)\right], \tag{A.7}$$

where $\lambda(t)$ is a stationary process.

REFERENCES

[1] J. Best, *Doubly stochastic processes: An approach for understanding central nervous system activity*, Proc. 3rd Int. Conf. Appl. Math. Simul. Model., (2009), pp. 155–158.

[2] P. R. Bouzas, M. J. Valderrama, and A. M. Aguilera, *On the characteristic functional of a doubly stochastic Poisson process: Application to a narrow-band process*, Appl. Math. Model., 30 (2006), pp. 1021–1032.

[3] P. C. Bressloff, *A stochastic model of intraflagellar transport*, Phys. Rev. E, 73 (2006), 061916.

[4] P. C. Bressloff, *Stochastic Processes in Cell Biology,* Springer, Berlin, 2014.

[5] D. R. Cox, *Some statistical methods connected with series of events*, J. R. Stat. Soc. B, 17 (1955), pp. 129–164.

[6] D. R. Cox and V. Isham, *Point Processes*, Chapman and Hall, London, 1980.

[7] D. J. Daley and D. Vere-Jones, *An Introduction to the Theory of Point Processes, Volume* I: *Elementary Theory and Methods*, Springer, Berlin, 2003.

[8] D. J. Daley and D. Vere-Jones, *An Introduction to the Theory of Point Processes, Volume* II: *General Theory and Structure*, Springer, Berlin, 2008.

[9] J. A. Deane, D. G. Cole, and J. L. Rosenbaum. *Localization of intraflagellar transport protein IFT52 identifies basal body transitional fibers as the docking site for IFT particles*, Current Biol., 11 (2001), pp. 1586–1590.

[10] C. W. Gardiner, *Handbook of Stochastic Processes*, Springer, Berlin, 2009.

[11] D. T. Gillespie, *Exact stochastic simulation of coupled chemical reactions*, J. Phys. Chem., 81.25 (1977), pp. 2340–2361.

[12] N. W. Goehring and A. A. Hyman, *Organelle growth control through limiting pools of cytoplasmic components*, Current Biol., 22 (2012), pp. R330–R339.

[13] J. Grandell. *Doubly Stochastic Process*, 1st ed., Springer-Verlang, New York, 1976.

[14] M. Kac, *On the distribution of certain Wiener functionals*, Trans. Amer. Math. Soc., 65 (1949), pp. 1–13.

[15] B. R. Karamched and P. C. Bressloff, *Delayed feedback model of axonal length sensing*, Biophys. J., 108 (2015), pp. 2408–2419.

[16] I. Katsura, *Determination of bacteriophage λ tail length by a protein ruler*, Nature, 327 (1987), pp. 73–75.

[17] J. P. Keener, *How Salmonella typhimurium measures the length of flagellar filaments*, Bull. Math. Biol., 68 (2006), pp. 1761–1778.

[18] M. Krumin and S. Shoham, *Generation of spike trains with controlled auto- and cross-correlation functions*, Neural Comput., 21 (2009), pp. 1642–1664.

[19] D. Lando, *On Cox processes and credit risky securities*, Rev. Derivatives Res., 2 (1998), pp. 99–120.

[20] K. F. Lechtreck, J. C. Van De Weghe, J. A. Harris, and P. Liu, *Protein transport in growing and steady-state cilia*, Traffic, 18 (2017), pp. 277–286.

[21] P. A. Lewis and G. S. Shedler, *Simulation of nonhomogeneous Poisson processes by thinning*, Naval Res. Logist., 26 (1979), pp. 403–413.

[22] Y. Liang, Y. Pang, Q. Wu, et al., *FLA8/KIF3B phosphorylation regulates kinesin-II interaction with IFT-B to control IFT entry and turnaround*, Dev. Cell, 30 (2014), pp. 585–597.
[23] S. B. Lowen and M. C. Teich, *Doubly stochastic Poisson point process driven by fractal shot noise*, Phys. Rev. A, 43 (1991), pp. 4192–4215.
[24] W. B. Ludington, K. A. Wemmer, K. F. Lechtreck, G. B. Witman, and W. F. Marshall, *Avalanche-like behavior in ciliary import*, Proc. Natl. Acad. Sci. USA, 110 (2013), pp. 3925–3930.
[25] W. B. Ludington, H. Ishikawa, Y. V. Serebrenik, A. Ritter, R. A. Hernandez-Lopez, J. Gunzenhauser, E. Kannegaard, and W. F. Marshall. *A systematic comparison of mathematical models for inherent measurement of ciliary length: How a cell can measure length and volume*, Biophys. J., 108 (2015), pp. 1361–1379.
[26] S. N. Majumdar, *Brownian functionals in physics and computer science*, Current Sci., 89 (2005), pp. 2076–2092.
[27] W. F. Marshall and J. L. Rosenbaum, *Intraflagellar transport balances continuous turnover of outer doublet microtubules: Implications for flagellar length control*, J. Cell Biol., 155 (2001), pp. 405–414.
[28] W. F. Marshall, H. Qin, M. R. Brenni, and J. L. Rosenbaum, *Flagellar length control system: Testing a simple model based on intraflagellar transport and turnover*, Mol. Biol. Cell, 16 (2005), pp. 270–278.
[29] W. F. Marshall, *How cells measure length on subcellular scales*, Trends Cell Biol., 25 (2015), pp. 760–768.
[30] A. E. Powell and M. Lenhard,*Control of organ size in plants*, Current Biol., 22 (2012), pp. R360–R367.
[31] B. Prevo, J. M. Scholey and E. J. G. Peterman, *Intraflagellar transport: Mechanisms of motor action, cooperation and cargo delivery*, FEBS J., (2017) 14068.
[32] B. E. A. Saleh and M. C. Teich, *Multiplied-Poisson noise in pulse, particle, and photon detection*, Proc. IEEE, 70 (1982), pp. 229–245.
[33] J. M. Scholey, *Intraflagellar transport*, Annu. Rev. Cell Dev. Biol., 19 (2003), pp. 423–443.
[34] S. Shinomoto and T. Yasuhiro, *Modeling spiking behavior of neurons with time-dependent Poisson processes*, Phys. Rev. E, 64 (2001), p. 041910.
[35] M. C. Teich and B. E. A. Saleh, *Inter-event-time statistics for shot-noise-driven self-exciting point processes in photon detection*, J. Opt. Soc. Amer., 71 (1981), pp. 771–776.
[36] M. C. Teich, C. Heneghan, S. B. Lowen, T. Ozaki, and E. Kaplan, *Fractal character of the neural spike train in the visual system of the cat*, J. Opt. Soc. Amer. A, 14 (1997), pp. 529–546.
[37] K. N. Wren, J. M. Craft, D. Tritschler, A. Schauer, D. K. Patel, E. F. Smith, M. E. Porter, P. Kner, and K. F. Lechtreck, *A differential cargo-loading model of ciliary length regulation by IFT*, Current Biol., 23 (2013), pp. 2463–2471.